

# A mineralogy of extrasolar silicate dust from 10- $\mu$ m spectra

J. E. Bowey<sup>1,2\*</sup> and A. J. Adamson<sup>1,3</sup>

<sup>1</sup>University of Central Lancashire, Preston PR1 2HE

<sup>2</sup>Department of Physics and Astronomy, University College London, Gower Street, London WC1E 6BT

<sup>3</sup>The UK Infrared Telescope (UKIRT), Joint Astronomy Centre, 660 N. A'ohoku Place, Hilo, HI 96720, USA

Accepted 2002 March 6. Received 2002 March 4; in original form 2001 March 26

## ABSTRACT

The 10- and 18- $\mu$ m spectroscopy of a variety of galactic environments reveals smooth bands which have been associated with (respectively) Si–O stretching and bending modes in amorphous silicates, since the spectra of crystalline silicates are narrow and highly structured. The standard approach to the interpretation of astronomical spectra is to assume that the silicates are amorphous and then to add in crystalline components (usually a single olivine followed by a pyroxene) to match fine structures in the data. Conversely, in this analysis we match the gross properties of the astronomical profiles – the full width at half-maximum (FWHM) and the wavelength of the peak ( $\lambda_c$ ) – with a mixture of crystalline silicates from different structural (and hence different spectral) classes and add a component of amorphous silicate only if there is too much structure in the simulation. We find that the narrow bands of crystalline grains could blend to form the broad 10- $\mu$ m bands observed. For all the environments included herein, if crystalline silicates are included in the mixture,  $\chi^2/n$  of the fits improves significantly (by factors of 1.3–4.4) and the number of silicon atoms required to model the spectra decreases by 30–50 per cent. Upper limits to the mass fraction of crystalline pyroxene increases with the FWHM of the profile from  $\sim$ 50 per cent in the sampled circumstellar environments to  $\sim$ 80 per cent in the Taurus molecular cloud (TMC) and its embedded young stellar objects (YSOs). Fine structures common to both the averaged spectra of laboratory silicates and astronomical profiles suggest that  $\leq$  10 per cent by mass of the silicates in circumstellar and star-forming environments could be partially crystalline hydrous (i.e. OH<sup>−</sup> containing) silicates similar to clays like talc and montmorillonite, but that these grains are absent from the ultraviolet-rich diffuse medium towards Cyg OB2 no. 12. In contrast, the relative abundance of submicrometre-sized crystalline olivine is insufficient ( $\leq$  25 per cent) in these circumstellar, diffuse-medium, molecular-cloud and YSO spectra to produce an 11.2- $\mu$ m emission or absorption feature. Using this method of spectral analysis, the mass fraction of amorphous silicate in these spectra could be as low as 17 per cent in the TMC and 0 per cent in some circumstellar environments.

**Key words:** astrochemistry – techniques: spectroscopic – circumstellar matter – stars: pre-main-sequence – dust, extinction – ISM: lines and bands.

## 1 INTRODUCTION

Interstellar silicates originate in post-main-sequence oxygen-rich stellar outflows and supernovae (e.g. Whittet 1992), are seen in the diffuse interstellar medium (ISM) and congregate in dense star-forming clouds, and their existence in these environments is well documented. Spatially unresolved spectroscopy of these environments reveals smooth 10- and 18- $\mu$ m bands which have been associated with amorphous silicates (e.g. Pégourié & Papoular

1985; Whittet et al. 1988; Bowey et al. 1998, hereafter Paper I). The narrow mean 10- $\mu$ m spectrum of massive young stellar objects (YSOs) has been fitted well with amorphous pyroxene (Jäger et al. 1994). However, fits with amorphous silicates to the 10- $\mu$ m profiles of dust in other environments (the diffuse ISM, the Taurus and Orion molecular clouds, T Tauri and Herbig AeBe stars) have been unsatisfactory (e.g. Jäger et al. 1994; Paper I). The match can be improved by the addition of iron metal and magnetite (Fe<sub>3</sub>O<sub>4</sub>) to enhance the opacity in the 2–8  $\mu$ m region (Ossenkopf, Henning & Mathis 1992). Since it is difficult to match the observations with a single amorphous silicate, 10- $\mu$ m spectra of molecular-cloud and

\*E-mail: jeb@star.ucl.ac.uk

low-mass YSO environments are frequently modelled with a profile shape (e.g. Hanner, Brooke & Tokunaga 1995, 1998; Paper I; Bowey & Adamson 2001, hereafter Paper II) or optical constants (Draine & Lee 1984) derived from observations of optically thin emission in the Trapezium<sup>1</sup> region of the Orion nebula (Forrest, Gillett & Stein 1977; Hanner et al. 1995).

In contrast, longer-wavelength ( $\sim 20\text{--}100\ \mu\text{m}$ ) *ISO* LWS and SWS spectra of newly formed oxygen-rich circumstellar dust indicate the presence of *crystalline* silicates (e.g. Waters et al. 1996). Monnier, Geballe & Danchi (1998) have presented time-resolved observations of  $10\text{-}\mu\text{m}$  circumstellar features with fine structures attributed to silicate dust, whilst Speck et al. (2000) assign a  $12.5\text{--}13\ \mu\text{m}$  band to highly polymerized silicate (in which most oxygen atoms are shared between two adjoining  $\text{SiO}_4$  tetrahedra) or  $\text{SiO}_2$  dust.

Evidence for crystalline silicates in the  $10\text{-}\mu\text{m}$  spectra of ‘old’ dust is limited to the polarization spectra of some embedded YSOs (e.g. AFGL 2591, Aitken et al. 1988; Smith et al. 2000), though a  $9.6\text{-}\mu\text{m}$  emission feature near  $\theta^2$  Ori A in the Orion nebula has been linked with evidence for crystalline pyroxenes and olivines at longer wavelengths (Cesarsky et al. 2000). Other fine structures in absorption spectra of deeply embedded YSOs have been associated with methanol (Skinner et al. 1992) and ammonia ices (Lacy et al. 1998). An  $11.2\text{-}\mu\text{m}$  band in the spectra of comets is ascribed to crystalline olivine, whilst other structure is associated with pyroxenes (e.g. Wooden et al. 1999).

This paper explores the possibility that crystalline and amorphous silicate dust may coexist in many galactic environments. It compares  $10\text{-}\mu\text{m}$  spectra of mixtures of crystalline and amorphous silicates with a carefully selected sample of the best available observations of newly formed and old circumstellar and interstellar dust. The observational data, all obtained with CGS3 on UKIRT, are taken from Papers I and II, and from Speck et al. (2000), and are described in Section 2. The negligible contribution of polycyclic aromatic hydrocarbons (PAHs) and ices to the observed profiles is discussed in Section 2.3. The standard approach to the interpretation of astronomical spectra is to assume that the silicates are amorphous (see Section 3) and then to add in crystalline components (usually a single olivine followed by a pyroxene) to match fine structures in the data. However, in Section 4 we select laboratory data for crystalline and amorphous silicates on the basis of cosmic elemental abundances, rather than on the shape of the spectrum; the laboratory data and methods are discussed in Section 4.1, the selection and spectral classification criteria are in Section 4.2 and the calculation methods are described in Sections 4.3 and 4.4. We match the gross properties of the astronomical profiles – the full width at half-maximum (FWHM) and the wavelength of the peak ( $\lambda_c$ ) with a mixture of crystalline silicates from different structural (and hence different spectral) classes and add a component of amorphous silicate only if there is too much structure in the simulation in Section 5. We look at the fine structure to deduce any other crystalline components (Section 5.2). The consequences of a mixed crystalline and amorphous mineralogy on the silicon abundance requirements for grain models and the mass fraction of crystalline and amorphous silicates are discussed in Section 6.

<sup>1</sup>The two Trapezium profiles were obtained with different beam sizes (probably  $\sim 11\text{--}22$  and  $5.5$  arcsec, respectively) and probably centred on different parts of the nebula. The profiles differ in both width and peak wavelength.

## 2 THE $10\text{-}\mu\text{m}$ OBSERVATIONS AND CONTINUA

### 2.1 Observations

Observations of diffuse-medium dust towards Cyg OB2 no. 12 and through the Taurus molecular cloud (TMC) to the field star Taurus-Elias 16 (Paper I) and towards the low-mass YSOs HL Tau and Taurus-Elias 7 (Haro 6-10 or GV Tau; Paper II) were obtained on 1993 November 7–8 using CGS3 at UKIRT. Details of the observations and reduction to flux spectra are given in Paper I. Since independent observations of HL Tau and Elias 7 by Hanner et al. (1998) contain the same fine structures (Fig. 1), we believe that the telluric cancellation for water vapour ( $\lambda \lesssim 8.2\ \mu\text{m}$ ), ozone ( $9.3\ \mu\text{m} \lesssim \lambda \lesssim 10.1\ \mu\text{m}$ ) and carbon dioxide ( $\lambda \gtrsim 13\ \mu\text{m}$ ) is excellent. The signal-to-noise ratios (s/n) of the derived optical depth spectra at  $9.7\ \mu\text{m}$ , close to the centre of the ozone feature, are given in Table 1. Speck et al. (2000) obtained  $10\text{-}\mu\text{m}$  spectra of 70 oxygen-rich asymptotic giant branch (AGB) stars which they classified according to the shapes of the feature: 35 had classic ‘ $9.7\text{-}\mu\text{m}$ ’ silicate features which were subdivided into classes A (7 stars), B (11 stars), C (12 stars) and D (5 stars) in order of increasing width; 11 had broader features with an emerging  $9.7\text{-}\mu\text{m}$  silicate bump, 15 had broad features with no bump, and 7 spectra were featureless. The spectra of CU Cep and U Aur are representative members of the narrow silicate feature groups A (FWHM  $\sim 2.5\ \mu\text{m}$ ) and B (FWHM  $\gtrsim 2.8\ \mu\text{m}$ ), respectively. The difference in the widths of these two groups is due to the enhanced optical depth of the  $\sim 11.0\text{-}\mu\text{m}$  shoulder in group B. The differences between spectra in group A are small:  $\lesssim 5$  per cent variation in the narrowness of the peak and the fine structure. Group B spectra show slightly more variation with changes in the relative proportions of the  $11\text{-}\mu\text{m}$  shoulder and main peak; in 5 out of the 11 members, the shoulder is as high as the main peak.

### 2.2 Derivation of silicate profiles

Since Cyg OB2 no. 12 and Elias 16 are obscured only by cold

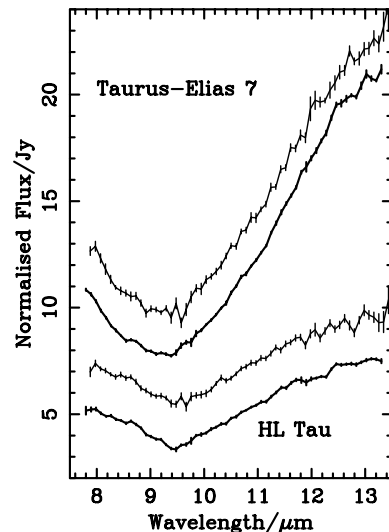


**Figure 1.** Comparison of fine structure in CGS3 observations of HL Tau and Elias 7 from Paper II (heavy lines) and Hanner et al. (1998) (light lines). The Hanner et al. data were normalized to the observations from Paper I and offset by  $+2.0\ \text{Jy}$  for clarity.

**Table 1.** Signal-to-noise ratio (s/n) at 9.7  $\mu\text{m}$ , silicate abundances and upper-limit optical depths and column densities for H<sub>2</sub>O, methanol and ammonia ices and for hexamethylenetetramine (HMT) residue in the 10- $\mu\text{m}$  silicate absorption spectra.

		H <sub>2</sub> O		Methanol		Ammonia		HMT				
$\lambda$ ( $\mu\text{m}$ )		3.0	$\sim 13$	9.8	9.0	10.0						
$\Delta\lambda$ ( $\mu\text{m}$ ) <sup>a</sup>		0.23	$\sim 5.3^b$	0.36	0.54	0.20						
$\sigma_{\text{int}} \times 10^{-20c}$		19	60	17	1900	5.0						
Source	s/n	$A_V$	$\tau^d$	$N_{\text{H}_2\text{O}} \times 10^{16f}$	$\tau_{\text{lib}}^e$	$\tau$	$N_{\text{meth}} \times 10^{16}$	$\tau$	$N_{\text{NH}_3} \times 10^{16}$	$\tau$	$N_{\text{HMT}} \times 10^{16}$	
Diffuse ISM	Cyg OB2 no. 12 <sup>h</sup>	41	10	$< 0.02^g$	$< 4.0$	$< 0.004$	–	–	–	$< 0.0067$	$< 2.7$	
TMC	Elias 16	10	22.3 <sup>i</sup>	1.60	190	0.32	$< 0.040$	$< 8.3$	$< 0.020$	$< 0.057$	$< 0.058$	$< 23$
YSO	Elias 7	65	6–10	$0.52 \pm 0.08$	63	0.10	$< 0.0054$	$< 1.2$	$< 0.032$	$< 0.092$	$< 0.0022$	$< 0.88$
YSO	HL Tau	61	23	0.85	100	0.17	$< 0.017$	$< 3.5$	$< 0.024$	$< 0.069$	$< 0.024$	$< 9.7$

<sup>a</sup>Mean wavelength and FWHM of feature measured from laboratory spectra by Hudgins et al. (1993).

<sup>b</sup>FWHM 4.5–5.3  $\mu\text{m}$  depending on the ice mixture.

<sup>c</sup>Integrated cross-section of band in  $\text{cm}^2 \mu\text{m}$  per molecule: H<sub>2</sub>O and methanol (Skinner et al. 1992); for NH<sub>3</sub> the effective band strength is  $1.1 \times \sigma_{\text{NH}_3}$ , since ratio of ammonia to H<sub>2</sub>O in this mixture is 1:10 (Lacy et al. 1998); HMT (Bernstein et al. 1995).

<sup>d</sup>H<sub>2</sub>O ice data from Whittet et al. (1988).

<sup>e</sup>Estimated from 3.0- $\mu\text{m}$  band depth.

<sup>f</sup>Units of column density are  $\text{cm}^{-2}$ .

<sup>g</sup>From Whittet et al. (1997).

<sup>h</sup>Values from paper I, except for NH<sub>3</sub>.

<sup>i</sup>Chiar et al. (1995).

absorbing dust, the continua of these objects were fitted using a reddened blackbody model (Paper I). YSOs HL Tau and Elias 7 have strong silicate absorption features, but their spectra are affected by emission from heated local dust. Hence, in Paper II the non-photospheric 10- $\mu\text{m}$  continua of HL Tau and Taurus-Elias 7 were estimated by fitting a disc model with radial power-law density and temperature indices and components of silicate emission and foreground absorption. For the details of the fitting procedure and comparison of the continua derived with different silicate profiles, we refer the reader to Paper II. The best fits were obtained with the Trapezium emissivity; fits with other profiles did not match  $\lambda_{\text{pk}}$  or the width of the profiles. The modelled 10- $\mu\text{m}$  emission of HL Tau contains optically thin silicate emission; that of Elias 7 is optically thick and featureless. Changes in the modelling emissivity affect the width of the silicate feature: fits obtained with  $\mu$  Cephei are 0.9 (HL Tau) and 1.0  $\mu\text{m}$  (Elias 7) narrower than the better fits obtained with the Trapezium. However,  $\lambda_{\text{pk}}$  and the fine structure in the profile remain the same with both models.

To obtain the circumstellar silicate profiles of CU Cep and U Aur, a photospheric continuum was first subtracted from the observations (see Speck et al. 2000); the remaining fluxes were divided by 250 and 225 K blackbodies scaled to the observations at 8.4  $\mu\text{m}$ . The resulting profiles of circumstellar, diffuse-medium, Taurus molecular-cloud and YSO dust are plotted in Fig. 2.

### 2.3 Fine structures due to PAHs and ices

Fine structures due to PAH emission are absent from the spectra of CU Cep and U Aur (Speck et al. 2000), the infrared spectra of Cyg OB2 no. 12 (Whittet et al. 1997), and the TMC sources (Whittet et al. 1988). The 12.3- $\mu\text{m}$  hydrogen 7–6 emission line was excluded before fitting the continua of Cyg OB2 no. 12 (see Paper I) and Elias 7. Frozen volatiles such as methanol and ammonia and photolysis residues such as hexamethylenetetramine (HMT, Bernstein et al. 1995) can produce narrow absorption features in the 10- $\mu\text{m}$  window. The upper (68 per cent confidence) limits of methanol and HMT optical depth were obtained by fitting a

Gaussian to the silicate absorption features of Elias 7 and HL Tau after subtracting the best-fitting emissivity to remove the silicate feature, and subtracting polynomials to remove wider-scale variations. The results, with those from Paper I for Elias 16 and Cyg OB2 no. 12, are listed in Table 1. Lacy et al. (1998) identified a 9.0- $\mu\text{m}$  band with a 2–10 per cent ammonia/H<sub>2</sub>O ice mixture in the strong ‘silicate’ absorption spectrum of the protostar NGC 7538 IRS 9. Therefore we also tabulate limits on the column density of NH<sub>3</sub> for the TMC sources; in all cases the upper limit is  $< 0.02$  per cent of the silicate column density (see Table 5). The H<sub>2</sub>O ice abundance is probably the best indicator of the degree of heating in each line of sight; H<sub>2</sub>O ice abundance and the optical depth of a 5.3- $\mu\text{m}$ -wide 13- $\mu\text{m}$  H<sub>2</sub>O ice libration feature which may be present in the TMC spectra (see Paper I) are estimated from the optical depth of the 3.0- $\mu\text{m}$  H<sub>2</sub>O ice feature. The peak of the broad H<sub>2</sub>O libration feature occurs longward of the Si–O bands (see Fig. 4 later). Hence, the question of whether the libration feature is present will not affect the inferred silicate mineralogy. The ratio of the methanol upper limits to the water ice abundance are  $< 4.4$  per cent (Elias 16),  $< 3.5$  per cent (HL Tau) and  $< 1.9$  per cent (Elias 7). HMT abundance limit correlates with the s/n of the spectrum. The ratio of H<sub>2</sub>O ice column density to silicate column density will be discussed later, in Section 6.1.1.

### 2.4 Sharpening of the silicate peak

A substantial fraction of the classic 10- $\mu\text{m}$  silicate spectra of O-rich AGB stars presented by Speck et al. contain a narrow ( $\Delta\lambda = 0.5 \mu\text{m}$ ) emission feature near the silicate peak which is larger than the errors:  $\sim 100, 82, 75, 40$  and  $85$  per cent of groups A, B, C, D and the broad + sil class, respectively, and the statistics of their observations of 39 O-rich supergiants are similar. In addition, some of the time-resolved observations of 10- $\mu\text{m}$  circumstellar silicate emission by Monnier et al. (1998) contain a similar feature which they attribute to the existence of ‘pure’ silicates. Moreover, our spectra of YSOs HL Tau and Elias 7

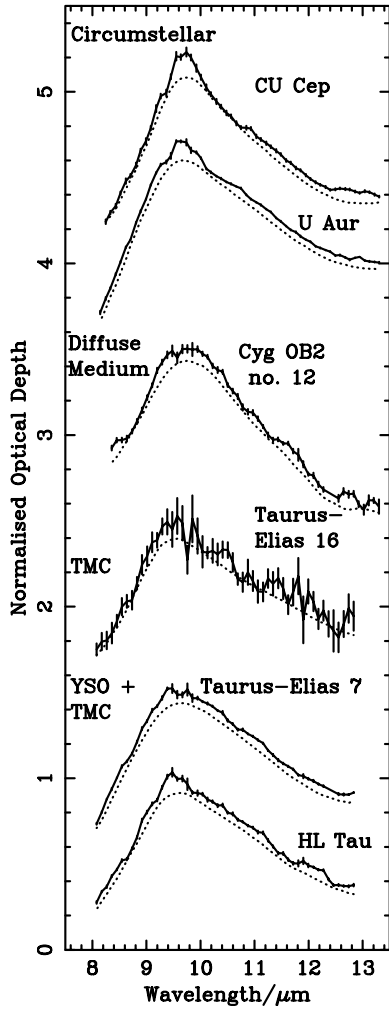


**Figure 2.** Astronomical 10- $\mu\text{m}$  profiles normalized to unity at the wavelength of their peaks (solid lines with error bars). Top to bottom: silicate emission features towards CU Cep and U Aur (Speck et al. 2000); silicate absorption towards Cyg OB2 no. 12, Taurus-Elias 16 (Paper I) and YSOs Taurus-Elias 7 and HL Tau (Paper II). The y-axis offsets are 0.0, 0.5, 1.5, 2.5, 3.7 and 4.2, respectively. Smoothed versions of the profiles (dotted lines) were subtracted from the observations to show up fine structure (see Fig. 7 in Section 5.2); these are offset from the observations by  $-0.05$  for clarity.

contain a feature at 9.4  $\mu\text{m}$  that is similar in shape to this and the 9.8- $\mu\text{m}$  ‘methanol’ feature observed in GL 2136 by Skinner et al. (1992). Independent observations of HL Tau and Elias 7 by Hanner et al. (1998) contain similar fine structures to our observations, but have lower  $s/n$ , especially in the region of the 9.3–10.1  $\mu\text{m}$  telluric ozone feature (Fig. 1), so the weak 9.4- $\mu\text{m}$  band is not discernible in their data. Sharpening of the peak is absent from the good spectrum of Cyg OB2 no. 12 and the low  $s/n$  spectrum of Elias 16 which contains no fine structure larger than the errors.

When the ‘sharp’ feature is observed it always occurs in *emission* in 10- $\mu\text{m}$  silicate emission spectra (see data in Speck et al. 1992) and in *absorption* in 10- $\mu\text{m}$  absorption spectra (see data in Skinner et al. 1992; Paper II; Cesarsky et al. 2000); if it were due to telluric ozone one would not see this correlation. Since silicate dust is common to all these environments, we propose that *crystalline* or partially crystalline silicates carry this and other fine structures.

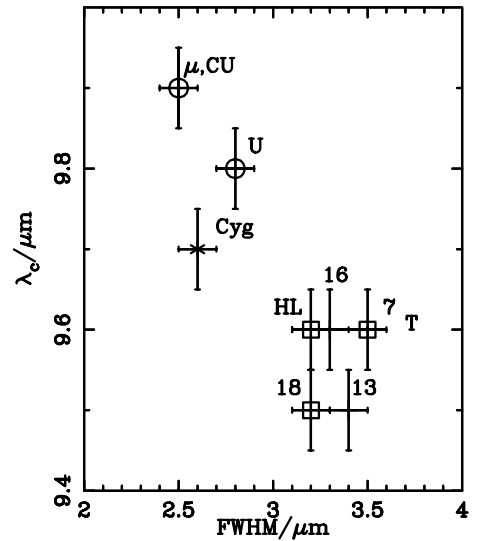


**Figure 3.** Effect of environment on full width at half-maximum (FWHM) and the central wavelength ( $\lambda_c$ ) of the normalized silicate profiles:  $\circ$ , circumstellar (CU Cep, U Aur,  $\mu$  Cephei; Russell, Soifer & Forrest 1975);  $\times$ , diffuse medium (Cyg OB2 no. 12);  $\square$ , YSO and TMC (HL Tau, Taurus-Elias 7 and 18) and Orion Trapezium (Forrest et al. 1975);  $+$ , quiescent TMC (Taurus-Elias 16 and 13).

**Table 2.** Normalized spectra of amorphous silicates (Blanco et al. 1993). Mixture Am is the arithmetic mean of the other spectra.

Group <sup>a</sup>	Name <sup>a</sup>	Stoichiometry	FWHM ( $\mu\text{m}$ )	$\lambda_{\text{pk}}$ ( $\mu\text{m}$ )
Olivines	Synthetic olivine	$(\text{Fe}_{0.6}\text{Mg}_{0.4})_2\text{SiO}_4$	2.1	9.8
	Synthetic cosmic silicate	$(\text{Fe}_{0.6}\text{Mg}_{0.4}\text{Al}_{0.035}\text{Ca}_{0.03}\text{Na}_{0.025})_2\text{SiO}_4$	2.3	9.9
	Olivine	$(\text{Mg}_{0.9}\text{Fe}_{0.1})_2\text{SiO}_4$	2.0	9.8
Pyroxene	Diopside	$[\text{X}]\text{SiO}_3^b$	2.0	9.6
?	Serpentine	$(\text{Mg}_6\text{Si}_4\text{O}_{10})(\text{OH})_8^c$	2.0	9.8
Mixture Am			2.2	9.9

<sup>a</sup>Strictly, mineral nomenclature depends on both the structure and the composition of the crystalline lattice, but these are amorphous samples. Here silicate group and nomenclature is determined by the stoichiometry.

<sup>b</sup>X = metal atom; Blanco et al. (1993) did not quote a formula. Typical composition of diopside is  $\text{MgCaSi}_2\text{O}_6$  (e.g. Ferraro 1982).

<sup>c</sup>Stoichiometry of the mineral before evaporation and recondensation. The spectrum of the amorphous condensate indicates an olivine stoichiometry (Bowey et al. 2000).

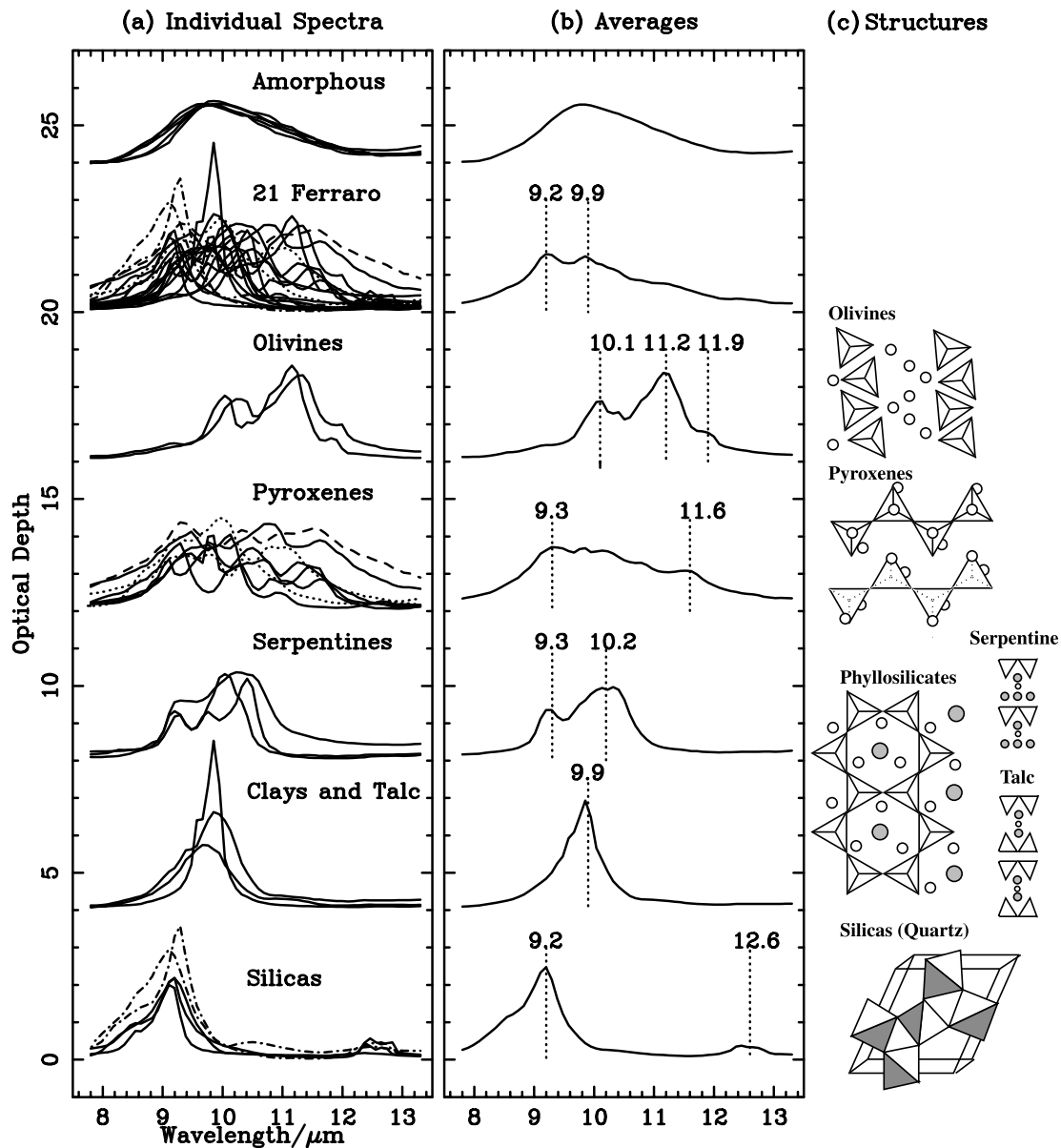


**Figure 4.** Spectral and structural characteristics of averaged spectral classes. (a) KBr spectra of individual members (Ferraro 1982): solid lines, Mg, Fe or  $\text{SiO}_2$  silicates; dashed lines, minerals containing Ca, Na and Al; dotted lines, minerals containing Ca; chain lines, hydrated  $\text{SiO}_2$  minerals. (b) Group averages: wavelengths of characteristic features are indicated; each group is offset by 4.0 from the one below it. (c) Mineral structures: tetrahedra and triangles represent top and side views of the  $\text{SiO}_4^{2-}$  groups, respectively; unshaded circles represent metal $^{2+}$  cations; and shaded circles represent hydroxyl  $\text{OH}^-$  anions. The serpentine and talc side views represent the stacking order of the silicate-ring layers, hydroxyl anions and cations. Silicas have a three-dimensional  $\text{SiO}_4^{2-}$  lattice. See Bowey et al. (2001) for side views of the olivine and pyroxene structures.

### 3 THE AMORPHOUS SILICATE INTERPRETATION

The central wavelength,  $\lambda_c$ , of the 10- $\mu\text{m}$  peak decreases from  $\geq 9.8 \mu\text{m}$  in circumstellar and diffuse-medium environments to  $9.6 \mu\text{m}$  in the TMC, whilst the FWHM increases from  $\sim 2.5$  to  $3.3 \mu\text{m}$  (Fig. 3). These changes in the profiles represent the effect of mixing grains from different sources and of chemical and physical processing on the older TMC and YSO silicates. The central wavelength of the 10- $\mu\text{m}$  peak ( $\lambda_c$ ) of amorphous olivines  $[(\text{Mg}_x, \text{Fe}_{1-x})_2\text{SiO}_4]$  occurs at  $9.8\text{--}9.9 \mu\text{m}$ , whilst amorphous pyroxenes  $(\text{Mg}_y, \text{Fe}_{1-y}\text{SiO}_3)$  peak at  $9.6 \mu\text{m}$  (e.g. Table 2).

Hence, we agree with Pégourié & Papoular (1985), who deduced

that circumstellar dust is rich in amorphous olivine and that amorphous pyroxene prevails in molecular clouds and YSOs. The greater width of the TMC profiles is due mainly to a  $\sim 2 \mu\text{m}$ -wide excess centred at  $11.5 \mu\text{m}$  which has been attributed to the shifted peak of larger micrometre-sized grains (e.g. Paper I). However, Bradley et al. (1999) show that such a feature exists in the spectra of (submicrometre-sized) glass with embedded metal and sulphides (GEMS). Here we also base our interpretation in terms of grain composition.

### 4 MIXED CRYSTALLINE AND AMORPHOUS SILICATES

Natural terrestrial silicates are crystalline solids (see Fig. 4c for

**Table 3.** The 21 crystalline mineral spectra from Ferraro (1982) that were included in mixture 21 Ferraro. Bullets indicate that a mineral is included in a mixture. The parameters of the crystalline and amorphous mixtures 21 Ferraro and I–V are given in the last 5 rows of the table. We expect the weighted mean mass absorption coefficient at  $\lambda_{\text{pk}}$ ,  $\bar{\kappa}(\lambda_{\text{pk}})$ , and  $\sigma_{\text{int}}$  to be accurate to  $\pm 15$  per cent.

Class	$\lambda_{\text{pk}}$ ( $\mu\text{m}$ )	$\tau_{\text{pk}}$ ( $\mu\text{m}$ )	$\bar{\kappa}(\lambda_{\text{pk}})^a$ ( $10^3 \text{ cm}^2 \text{ g}^{-1}$ )	$\bar{m}_r/r_{\text{O:Si}}^b$	$\sigma_{\text{int}} \times 10^{-20c}$	Mixture							
						Mineral spectra included in 21 Ferraro	I	II	III	IV	V		
Olivines	11.2	2.3	8.9	41.5	270	(Mg,Fe) <sub>2</sub> SiO <sub>4</sub>	Olivine–chrysolite	●	●				●
						(Fe,Mg) <sub>2</sub> SiO <sub>4</sub>	Hortonolite	●	●				●
Pyroxenes	9.3	1.7	4.9	37.1	160	MgSiO <sub>3</sub>	Enstatite	●	●	●	●	●	●
						MgSiO <sub>3</sub>	Bronzite	●	●	●	●	●	●
						(Mg,Fe)SiO <sub>3</sub>	Hypersthene	●	●	●	●	●	●
						(Mg,Fe) <sub>7</sub> Si <sub>8</sub> O <sub>22</sub> (OH) <sub>2</sub>	Anthophyllite	●	●	●	●	●	●
						MgCaSi <sub>2</sub> O <sub>6</sub>	Diopside	●	●	●	●	●	●
						(Mg,Fe,Ca)(Mg,Fe)-Si <sub>2</sub> O <sub>6</sub>	Pyroxene <i>var.</i> pigeonite	●	●	●	●	●	●
						$\alpha$ -CaSiO <sub>3</sub>	Wollastonite	●	●	●	●	●	●
						(Ca,Na)(Mg,Fe,Al)-(Si,Al) <sub>2</sub> O <sub>6</sub>	Augite	●	●	●	●	●	●
Serpentines	10.2	2.0	5.3	56.0	220	Mg <sub>3</sub> Si <sub>2</sub> O <sub>5</sub> (OH) <sub>4</sub>	Antigorite	●	●				●
						Mg <sub>3</sub> Si <sub>2</sub> O <sub>5</sub> (OH) <sub>4</sub>	Chrysotile	●	●				●
						(Mg,Fe) <sub>3</sub> Si <sub>2</sub> O <sub>5</sub> (OH) <sub>4</sub>	Serpentine	●	●				●
CIT minerals	9.9	2.9	9.6	38.4	150	3MgO · 4SiO <sub>2</sub> · H <sub>2</sub> O	Talc	●	●				
						Mg <sub>3</sub> Si <sub>4</sub> O <sub>10</sub> (OH) <sub>2</sub>	Stevensite	●	●				
						Mg <sub>2</sub> Si <sub>3</sub> O <sub>8</sub> ·2H <sub>2</sub> O	Magnesium silicate, hydrated	●	●				
Silicas	9.2	2.5	16	33.5	280	SiO <sub>2</sub>	Quartz						
						SiO <sub>2</sub>	Fumed silica						
						SiO <sub>2</sub> · xH <sub>2</sub> O	Silica, hydrated						
						SiO <sub>2</sub> ·nH <sub>2</sub> O	Opal						
						SiO <sub>2</sub>	Micronized amorphous silica						
Amorphous	9.8	1.0	2.6	40.8	45	(see Table 2)	(see Table 2)		●	●	●	●	●
Amorphous fraction, $x$ (per cent)							0	0	50	50	25	50	
$\lambda_{\text{pk}}$ ( $\mu\text{m}$ )							9.2	9.9	9.9	9.9	9.9	10.0	
$\bar{\kappa}(\lambda_{\text{pk}})$ ( $10^3 \text{ cm}^2 \text{ g}^{-1}$ )							6.7	5.6	4.1	3.7	4.3	3.6	
$\bar{m}_r/r_{\text{O:Si}}^b$							39.5	41.4	47.3	43.3	41.8	44.7	
$\hat{\sigma}_{\text{int}}$ ( $10^{-20} \text{ cm}^2 \mu\text{m Si-O}^{-1}$ )							120	95	70	71	83	78	

<sup>a</sup>For each group  $\bar{\kappa}$  is represented by that for a single mineral: Olivines – olivine (Koike et al. 1993); Pyroxenes – mean of clinopyroxene ( $5.3 \times 10^3$ ) and orthopyroxene ( $4.5 \times 10^3$ ) values (Koike et al. 1993); Serpentine – serpentine (Koike et al. 1982); CIT minerals – montmorillonite (Koike et al. 1982); Silicas – fused quartz (Koike & Shibai 1994); Amorphous – mean of amorphous olivine ( $2.3 \times 10^3$ ) and diopside ( $4.0 \times 10^3$ ) mass extinction coefficients weighted 4:1 according to olivine to pyroxene ratio (Koike & Tsuchiyama 1992; Koike et al. 2000).

<sup>b</sup> $\bar{m}_r/r_{\text{O:Si}}$  is the relative molecular mass of the silicate per Si–O bond.

<sup>c</sup>Units of  $\sigma_{\text{int}}$  are  $\text{cm}^2 \mu\text{m Si-O}^{-1}$ .  $\hat{\sigma}_{\text{int}}$  is the integrated cross-section of the normalized averages.

structures) in which the  $\text{SiO}_4^{2-}$  ions are separate (*olivines*) or are linked together via shared oxygen atoms to form anionic chains (*pyroxenes*) which are charge-balanced by metal cations. The phyllosilicates are formed of layers of joined silicate rings with metal cations and hydroxyl anions. Three-dimensional *framework silicates* are *silicas* formed entirely of  $\text{SiO}_2$  unless some  $\text{Si}^{4+}$  is replaced by  $\text{Al}^{3+}$  to provide other cation sites. Minerals within these groups contain different cations, e.g. in the olivine *solid solution series*  $\text{Mg}^{2+}$  are replaced with  $\text{Fe}^{2+}$ . The ratio of the metal cations in silicates with olivine and pyroxene stoichiometry has little effect on the spectra of *amorphous* silicates. However, the 10- $\mu\text{m}$  spectra of *crystalline* silicates from the same solid solution series vary (Fig. 4a); this has been the cause of the largest discrepancies between the 10- $\mu\text{m}$  spectra of apparently identical crystalline silicates (particularly olivines and serpentines) in the astronomical literature (Bowey, Adamson & Speck 2000).

#### 4.1 Laboratory spectra

To ensure consistency in mineral nomenclature and laboratory technique, the spectra of crystalline and amorphous silicates for use in comparisons with the astronomical data were each obtained from a single publication. The spectra of amorphous silicates (Blanco et al. 1993) were of 150–300 Å-sized condensates on KRS-5 substrates (see Stephens et al. 1995); the properties of the samples and the resulting spectra are listed in Table 2 and plotted in Fig. 4(a), respectively. Data for crystalline silicates were selected from Ferraro’s (1982) 2–40  $\mu\text{m}$  spectral atlas of 214 silicates, which is the most coherent data base available. These are of natural minerals which were ground and embedded in KBr pellets.

Estimates of the mass absorption coefficient,  $\kappa$ , are given by

$$\kappa = \frac{S}{M} \ln \frac{1}{T}, \quad (1)$$

where  $S$  is the surface area of a (disc-shaped) KBr pellet,  $M$  is the mass of mineral embedded and  $T$  is the measured transmittance.

The implicit assumption in equation (1) is that all the grains are in the Rayleigh size limit so that the measured absorption features are due to all the sample mass. Grains and clumps larger than the Rayleigh limit scatter the light or completely absorb it, thereby increasing the overall opacity and reducing the contrast in strong features such as the 10- $\mu\text{m}$  Si–O stretch.<sup>2</sup> Hence, the opaque clumps and larger grains contain most of the mass, whilst the small grains produce most of the absorption feature, and the measured mass absorption coefficient is lower than the true value. Consequently, when the data are applied to astronomical observations, more mass is required to match observational data than is actually present.

Ferraro’s pellet density and grain size (probably  $< 3 \mu\text{m}$ ) were sufficient to produce repeatable spectra and therefore must have contained a sufficient number of small grains to obtain good spectral contrast. Mass absorption coefficients, sample masses and grain size distributions are unrecorded. Estimates of the mass absorption coefficient at the wavelength of the Si–O peak were obtained from logarithmic plots by (Koike, Hasegawa & Hattori 1982; Koike & Tsuchiyama 1992; Koike, Shibai & Tsuchiyama 1993; Koike & Shibai 1994; Koike et al. 2000). The contrast in the 10- $\mu\text{m}$  optical depth spectra of individual minerals in both catalogues is the same to  $\leq 5$  per cent. The difference in wavelength between KBr spectra and absorption spectra derived from reflectance measurements with Mie theory (known as the ‘KBr shift’) is negligible ( $\leq \pm 0.05 \mu\text{m}$ ) in comparison to the shifts produced by mineralogical differences between silicates (Speck, Hofmeister & Barlow 1999; Bowey et al. 2000; Hofmeister et al. 2000). The ‘KBr shift’ is also insignificant in comparison to the modelled effect of grain shape on strong peaks<sup>3</sup> such as the Si–O stretch (Fabian et al. 2001). Powdered samples (and presumably astronomical grains) include a range of grain sizes and shapes. The advantage of using data for particulates is that a wider variety of minerals have been studied using this method.

#### 4.2 Selection and classification of crystalline silicates

Some 39 minerals within Ferraro’s sample are composed only of highly depleted cosmically abundant elements (O, Si, Fe, Mg, Al, H in  $\text{H}_2\text{O}$  and Ca; Anders & Grevesse 1989). Al-rich silicates [ten framework silicates, five phyllosilicates, two pyroxenes and allophane ( $\text{Al}_2\text{SiO}_5 \cdot n\text{H}_2\text{O}$ )] were excluded from the final selection because Al is expected to condense into  $\text{Al}_2\text{O}_3$  (Gail & Sedlmayr 1986) and Al abundance  $\leq 0.1 \times \text{Mg}$  abundance (Anders & Grevesse 1989). The 21 crystalline minerals, listed in Table 3 and plotted in Fig. 4(a), consist mainly of Mg- and Fe-rich olivines, pyroxenes and hydrous ( $\text{OH}^-$ ) silicates and silicas ( $\text{SiO}_2$  minerals); the included Ca-, Al- and Na-bearing pyroxenes wollastonite and augite are found in meteorites.

The spectra of crystalline minerals listed in Table 3 were sorted into olivine, pyroxene, serpentine, clay/talc (CIT) and silica classes

<sup>2</sup> In severely saturated spectra the measured band profile has a flat top and any observed fine structure is due to detector noise (see Hofmeister et al. 2000 for a full discussion).

<sup>3</sup> In scattering theory, grains are typically modelled as spheres (Mie theory), infinitely long cylinders or ellipsoids. Perfectly amorphous silicate grains are spheroidal. However, *by definition* crystals can take on a range of crystal shapes which are specific to each mineral, of which *none* are spherical, ellipsoidal, or cylindrical.

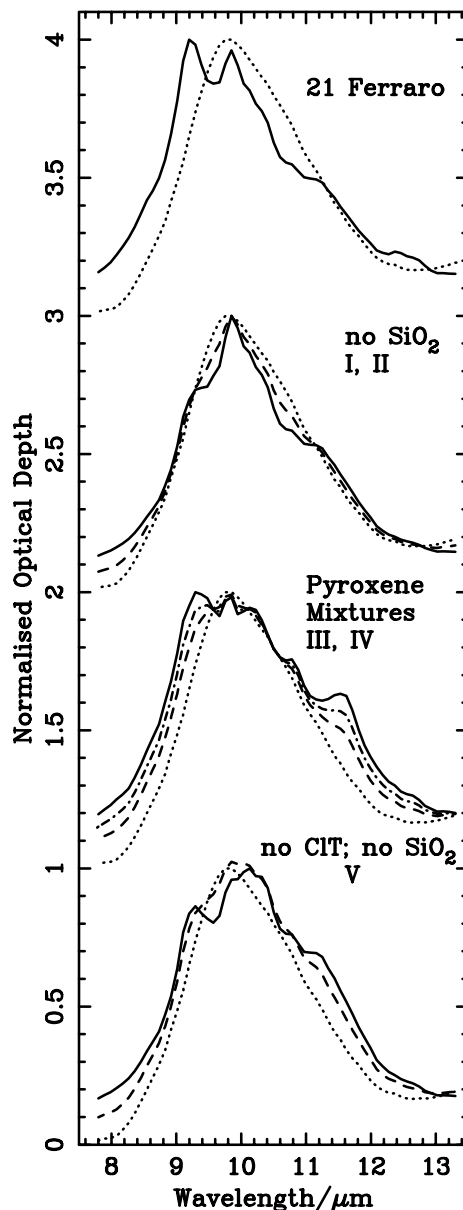


**Figure 5.** The effect of varying the components of a crystalline and amorphous mixture. Top to bottom: 21 Ferraro; the same excluding silicas; mixtures including only pyroxenes; and 21 Ferraro excluding talc, clays and silicas. Crystalline fraction: 100 per cent – solid line (I); 75 per cent – chain line (IV); 50 per cent – dashed line (II, III, V); 0 per cent – dotted line (Am). The y-axis offsets are 0.0, 1.0, 2.0 and 3.0.

according to their structural and spectral characteristics. The range of spectral properties within a class and the lattice structures are shown in Figs 4(a) and (c). The phyllosilicate group were subdivided into physically and hence spectrally distinct serpentine and clay/talc (CIT) classes. In the serpentine class layers of silicate rings point in the same direction and are separated by successive layers of hydroxyl ( $\text{OH}^-$ ) anions, metal<sup>2+</sup> cations and a second hydroxyl layer (see Fig. 4c). Minerals in the CIT group have structures similar to that of talc with the apices of the silicate tetrahedra pointing towards the hydroxyl and cation layers in a cationic sandwich with the ‘butter’ replaced by hydroxyl ions. Weaker van der Waals forces hold neighbouring layers of silicate rings together.

**Table 4.** Fraction of each mineral component by mass obtained with equation (A5) and stoichiometry of mixtures compared with interstellar depletion measurements by Snow & Witt (1996). Values are normalized to Si abundance (= 1). The term ‘metal’ is used in the chemical sense.  $O_{\text{hyd}}$  is the oxygen contained in  $\text{H}_2\text{O}$  or  $\text{OH}^-$ .

Average	Fraction by mass per cent						Stoichiometry relative to Si		
	$m_{\text{f,Am}}$	$m_{\text{f,ol}}$	$m_{\text{f,py}}$	$m_{\text{f,serp}}$	$m_{\text{f,CIT}}$	$m_{\text{f,SiO}_2}$	Metal	$O_{\text{total}}$	$O_{\text{hyd}}$
Am	100	0.0	0.0	0.0	0.0	0.0	1.7	3.6	0.0
21 Ferraro	0.0	19	32	20	9.1	21	0.84	3.2	0.49
Olivines	0.0	100	0.0	0.0	0.0	0.0	2.0	4.0	0.0
Pyroxenes	0.0	0.0	100	0.0	0.0	0.0	0.99	3.0	0.0
Serpentines	0.0	0.0	0.0	100	0.0	0.0	1.5	4.5	2.0
CIT minerals	0.0	0.0	0.0	0.0	100	0.0	0.72	3.1	0.60
Silicas <sup>a</sup>	0.0	0.0	0.0	0.0	0.0	100	0.0	2.4	0.40
I	0.0	25	39	25	11	0.0	1.3	3.5	0.54
II	37	16	25	16	6.9	0.0	1.4	3.6	0.37
III	40	0.0	60	0.0	0.0	0.0	1.2	3.2	0.0
IV	17	0.0	83	0.0	0.0	0.0	1.1	3.1	0.0
V	31	19	30	20	0.0	0.0	1.4	3.6	0.38
Interstellar							2.7 <sup>b</sup>	7.4	

<sup>a</sup>For Silica, hydrated ( $\text{SiO}_2 \cdot x \text{H}_2\text{O}$ ) and opal ( $\text{SiO}_2 \cdot n \text{H}_2\text{O}$ ), we assume  $x = n = 1$ .

<sup>b</sup>Mg + Fe abundances: [Mg] = 1.1, [Fe] = 1.6.

Spectral variation between minerals in most classes is due mainly to variation in the metals included in the structure. For example, the replacement of some  $\text{Mg}^{2+}$  with  $\text{Fe}^{2+}$  distorts the lattice because  $\text{Fe}^{2+}$  has a larger ionic radius and larger mass. Consequently the change in the silicate lattice alters the frequency of the spectral features. In other cases spectral differences result from the shape of the larger silicate lattice. For example, the spectrum of chrysotile serpentine has three peaks at  $10 \mu\text{m}$  because the silicate layers form cylinders, whilst antigorite which forms wavy layers has only two peaks. For a random selection of grains of olivine type the spectrum will result from grains with different Mg:Fe ratios. Therefore to mimic the effect of mixing on a class of silicates from diverse astronomical sources we average the available laboratory spectra. In the averages (Fig. 4b) the features blend and extreme spectral characteristics of individual members are smoothed out.

### 4.3 Simulation of crystalline mixtures

We aim to simulate the shape of a  $10\text{-}\mu\text{m}$  feature produced by mixtures of crystalline minerals by the use of Ferraro’s data for particulates with the minimum of assumptions (we do not consider grain size). The mean optical depth spectra of  $n$  crystalline minerals were calculated from Ferraro’s unnormalized optical depth spectra:

$$\bar{\tau}(\lambda) = \frac{1}{n} \sum_{i=1}^n \tau_i(\lambda). \quad (2)$$

The averages of Ferraro’s unnormalized spectra of the olivine, serpentine, clay/talc and silica groups are slightly broader than those of individual members but otherwise resemble them. However, in the pyroxene series the narrow peaks of individual chain silicates occur at a range of wavelengths, and their individual structures disappear, to be replaced by a single band of  $\text{FWHM} = 3.1 \mu\text{m}$ , which is broader than the profiles of individual amorphous silicates ( $2.0\text{--}2.3 \mu\text{m}$ ; Table 2) and the average spectrum of the amorphous silicates ( $\text{FWHM} = 2.2 \mu\text{m}$ ; Fig. 5). Thus an astronomical  $10\text{-}\mu\text{m}$  profile may hide a considerable fraction of crystalline pyroxenes.

In comparison to the individual spectra of the 21 crystalline minerals, the average spectrum, 21 Ferraro, is remarkably smooth and broad. The most prominent fine structures are the main and

secondary peaks at  $9.2$  and  $9.9 \mu\text{m}$ , respectively (Figs 4b and 5). The  $9.2\text{-}\mu\text{m}$  peak is due primarily to the very strong  $9.2\text{-}\mu\text{m}$  band of the silicas, whilst the  $9.9\text{-}\mu\text{m}$  peak coincides with that of the average of the amorphous silicates. Excluding the silicas to produce mixture I reduces the  $9.2\text{-}\mu\text{m}$  peak to a shoulder produced by the pyroxenes and serpentines.

The contrast in the  $10\text{-}\mu\text{m}$  optical depth spectra of individual minerals in the Ferraro (1982) and Koike catalogues (Koike et al. 1982; Koike & Tsuchiyama 1992; Koike et al. 1993; Koike & Shibai 1994; Koike et al. 2000) is the same to  $\leq 5$  per cent. Differences between members within a group are accounted for in equation (2). Therefore for each mineral class we adopt a measurement of the mass absorption coefficient of a single mineral at the wavelength of the Si–O peak,  $\bar{\kappa}(\lambda_{\text{pk}})$ , for the class (see Table 3). The integrated cross-section of the band per Si–O bond,  $\sigma_{\text{int}}$ , is given in Table 3. Mass fractions due to each spectral class are listed with the stoichiometry of the mixtures in Table 4. Details of the calculations are in Appendix A. Given that  $\bar{\kappa}(\lambda_{\text{pk}})$  is a representative value for each group and the experimental uncertainties, we expect this and the derived band cross-sections,  $\sigma_{\text{int}}$ , to be accurate to within  $\pm 15$  per cent.

### 4.4 Mixtures with an amorphous component

The published spectra of amorphous silicates were already normalized at  $\lambda_c$ . Hence, the mean optical depth spectrum of the five spectra of amorphous silicates (mixture Am) was obtained from these *normalized* data. The FWHM and  $\lambda_c$  of mixture Am (Figs 4b and 5) are similar to those of the amorphous olivines listed in Table 2.

Mixtures of crystalline and amorphous silicates were simulated by normalizing the simulated spectra of the crystalline mixtures to unity before calculating the mean of mixture Am and the appropriate crystalline mixture in the proportions required to produce the best match to the astronomical spectra. Hence, in terms of optical depth, if mixture Z is composed of  $x$  per cent amorphous mixture Am and  $(1 - x)$  per cent crystalline mixture Y, then the normalized optical depth of mixture Z at wavelength  $\lambda$ ,  $\tau_Z(\lambda)$ , is given by

$$\tau_Z(\lambda) = \frac{x}{100} \tau_{\text{Am}}(\lambda) + \left(1 - \frac{x}{100}\right) \tau_Y(\lambda), \quad (3)$$

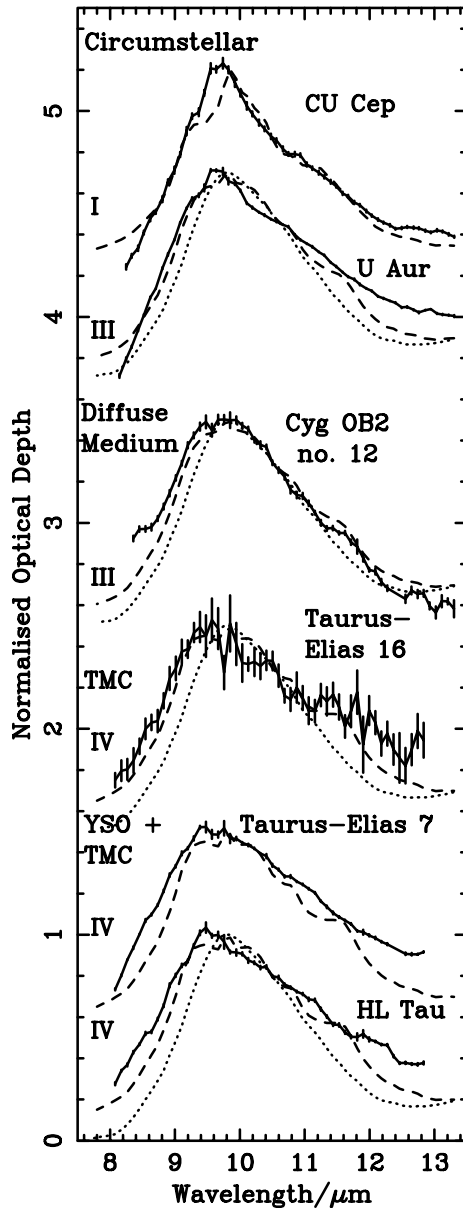


**Figure 6.** Matching FWHM and  $\lambda_c$  of the normalized astronomical silicate profiles with mixtures I–IV of crystalline and amorphous silicates (dashed line) and the average of the amorphous silicates (dotted line). See Fig. 2 for the y-axis offsets and Tables 2 and 3 for the components of mixtures I–IV.

and similarly the weighted mean mass absorption coefficient is

$$\bar{\kappa}(\lambda) = \frac{x}{100} \bar{\kappa}_{\text{Am}}(\lambda) + \left(1 - \frac{x}{100}\right) \bar{\kappa}_{\text{Y}}(\lambda). \quad (4)$$

In general the amorphous fraction smooths out fine structure in the mixtures (Fig. 5). However, if the wavelength of the peak of the amorphous minerals is substantially different from that of the crystalline component, it also shifts the peak of the combination as in mixture V.

Estimates of the integrated cross-sections and mass fractions were obtained in the same way as for the crystalline silicates (see Appendix A2) by replacing the spectral classes with the appropriate fractions of the normalized spectra of the crystalline and amorphous silicate mixtures. The approximate stoichiometries of the silicate mixtures are compared with measurements of interstellar depletions (Snow & Witt 1996) in Table 4. In all the

mixtures the ratio of metal:Si:O abundances falls within the depletions (relative to Si = 1.0) observed in the diffuse medium.

## 5 MINERALOGY OF ASTRONOMICAL SILICATES

The standard approach to the interpretation of astronomical 10- $\mu\text{m}$  profiles is to assume that the silicates are amorphous and then to add in crystalline components (usually a single olivine followed by a pyroxene) to match fine structures in the data. Conversely, in this analysis we match the gross properties of the astronomical profiles – the full width at half-maximum (FWHM) and the wavelength of the peak ( $\lambda_c$ ) – with a mixture of crystalline silicates which includes a range of minerals from each spectral class and add an amorphous component if there is too much structure in the simulation. Finally we look at the fine structure to deduce any other crystalline components. The presence of bands due to grain mantle components was ruled out in Section 2.3.

### 5.1 Matching $\lambda_c$ and FWHM

We matched  $\lambda_c$  and FWHM by ‘eye’. Mixture 21 Ferraro (see Table 3 and Fig. 4) is made up of the 21 minerals in Ferraro’s catalogue which best represent the possible interstellar compositions (see Section 4.2). However, there is no evidence of the strong 9.2- $\mu\text{m}$  silica peak in the astronomical profiles so the silicas were excluded to form mixture I. In the same manner, starting from mixture I, successive spectral classes were removed by inspection to improve the overall match. If excess fine structure remained in the simulation, a fraction (25, 50, or 75 per cent, by optical depth) of amorphous silicate was added to produce a smoother spectrum; therefore the resolution in the degree of crystallinity of the astronomical profiles is only 25 per cent.

The observations are plotted with the most similar laboratory mixtures in Fig. 6. In Table 5 we compare  $\chi^2/n$  and the silicon included in silicates of the preferred matches with those for the amorphous mixture, Am. Values of  $\chi^2/n$  are large because error bars represent uncertainties in telluric transmission, rather than the composition. We do not claim that these matches uniquely determine the detailed makeup of the grain material. However, some general conclusions can be drawn: in *all* cases the inclusion of crystalline minerals produces significantly better fits (by factors of 1.3 to 4.4) than those with only amorphous silicates.

The overall profile of circumstellar dust around CU Cep is reproduced by 100 per cent crystalline mixture I; the source of the unmatched excess shortward of the peak will be discussed in Section 5.2. The widths of the other spectra are matched better by mixtures of crystalline pyroxenes and amorphous silicates. Dust surrounding U Aur and diffuse-medium dust towards Cyg OB2 no. 12 are approximated by mixture III. For Cyg OB2 no. 12  $\chi^2/n$  for the match with mixture III is 26, *significantly* better than that with mixture Am for which  $\chi^2/n = 79$ . A larger (75 per cent) proportion of crystalline pyroxene (mixture IV) is required to fit the FWHM of TMC silicates towards Taurus-Elias 16;  $\chi^2/n$  of the crystalline and amorphous mixture is 3.2 instead of 14 for the amorphous silicates. Mixture IV also provides the best match to the absorption profiles of the YSOs Elias 7 and HL Tau. However, the smoothness of the Elias 7 and HL Tau spectra suggests that more than 17 per cent of the absorption is due to amorphous grains, or that the grains are so large that much of the fine structure is not revealed within the 10- $\mu\text{m}$  band.

**Table 5.** The  $\chi^2/n$ , silicate band column density ( $N_{\text{Si-O}}$ ) and silicon atom column densities ( $N_{\text{Si}}$ ) of the crystalline and amorphous silicate matches compared with values for the matches to the average of the amorphous silicates. The fraction of silicon atoms in the amorphous and crystalline components of the mixtures are also given. The optical depth resolution in the degree of crystallinity of the mixtures is 25 per cent. Mixture I is 100 per cent crystalline silicate; mixtures III and IV are formed of 40 and 17 per cent amorphous silicate by mass, respectively (see Table 4 for the other mixtures).

Environment	Source	$\tau_{\text{sil}}$	Amorphous silicate				Crystalline and amorphous silicate mixture				
			$\chi^2/n$	$N_{\text{Si-O}}$ $\times 10^{16} \text{ cm}^{-2}$	$N_{\text{Si}}^a$ $\times 10^{16} \text{ cm}^{-2}$		$\chi^2/n$	$N_{\text{Si-O}}$ $\times 10^{16} \text{ cm}^{-2}$	$N_{\text{Si}}$	$f(N_{\text{Si}})_{\text{Am}}$ (per cent)	$f(N_{\text{Si}})_{\text{Cryst}}$ (per cent)
Circumstellar	CU Cep	2.0	50	1100	310	I	39	520	170	0.0	100 <sup>b</sup>
Circumstellar	U Aur	1.5	3100	1000	280	III	1300	630	200	28	72
Diffuse ISM	Cyg OB2 no. 12	0.62	79	380	110	III	26	240	75	28	72
TMC	Taurus-Elias 16	0.81	14	560	160	IV <sup>c</sup>	3.2	300	97	11	89
YSO	Taurus-Elias 7	1.7	2800	1300	360	IV <sup>c</sup>	770	700	230	11	89
YSO	HL Tau	1.1	990	780	220	IV <sup>c</sup>	247	420	140	11	89

<sup>a</sup> $N_{\text{Si}} = N_{\text{Si-O}}/r_{0,\text{Si}}$ ;  $r_{0,\text{Si}}$  values for each mixture are given in Table 4.

<sup>b</sup>Number fraction of silicon atoms in each component: 18 per cent in olivines, 44 per cent in pyroxenes, 23 per cent in serpentines, 15 per cent in CITs.

<sup>c</sup>Owing to their large FWHMs, the lowest  $\chi^2/n$  for U Aur ( $\chi^2/n = 900$ ), Elias 7 (450), 16(2.1) and HL Tau (144) are obtained with the 100 per cent crystalline pyroxene mixture. However, the fine structures in these observations are insufficient for this to be the preferred match.

## 5.2 Fine structure

To identify fine structures in the data with plausible silicate carriers, the smoothed profiles shown in Fig. 2 were subtracted from the laboratory averages and high s/n astronomical profiles. The residuals are plotted in Fig. 7. Fine structures in the observations are considered genuine if they are larger than the estimated errors and are defined by more than three data points.

Relatively strong, narrow features are present in the CU Cep ( $\tau \sim 0.26$ ) and U Aur ( $\tau \sim 0.14$ ) residuals at  $\sim 9.8 \mu\text{m}$ . The feature is similar in shape and intensity to the  $9.9\text{-}\mu\text{m}$  band of the clay/talc (CIT) minerals in laboratory residuals I and II (Tables 2 and 3). Talc has weaker bands at other wavelengths. The strongest feature in the near-infrared is the  $\text{OH}^-$  band at  $2.719 \mu\text{m}$  (FWHM  $\approx 0.005 \mu\text{m}$ ); the ratio of the absorbances is  $\tau_{\text{OH}^-}/\tau_{9.9} \sim 0.16$ .<sup>4</sup> Hence, for CU Cep,  $\tau_{\text{OH}^-} \sim 0.04$ . If the  $9.9\text{-}\mu\text{m}$  peak were due to a montmorillonite clay, there could be a peak due to interstitial  $\text{H}_2\text{O}$  at  $2.912 \mu\text{m}$  (FWHM  $\sim 0.25 \mu\text{m}$ ) for which  $\tau_{\text{H}_2\text{O}}/\tau_{9.9} \lesssim 0.4$ ; for CU Cep,  $\tau_{\text{OH}^-} \sim 0.1$ . If  $\text{H}_2\text{O}$  ice were present, this band would appear as a weak shoulder on the  $3.0\text{-}\mu\text{m}$  ice band.

In the  $10\text{-}\mu\text{m}$  residuals of Elias 7 and HL Tau, weaker ( $\Delta\tau \lesssim 0.08$ ) features that are similar in shape to the CIT band are indicated at  $9.4 \mu\text{m}$  (shaded peaks in Fig. 7). If talc is rendered amorphous by prolonged grinding<sup>5</sup> (Filio et al. 1994), this band shifts to  $9.5 \mu\text{m}$  (Farmer 1958), and it also occurs at  $9.5 \mu\text{m}$  in the spectra of hydrous amorphous  $\text{MgSiO}$  smokes (see Nuth, Donn & Nelson 1986). However, no shift results from the substitution of  $\text{Fe}^{2+}$  for  $\text{Mg}^{2+}$  or Al for Si (Farmer 1958). Hence, the grains responsible for the excess shortward of the  $9.8\text{-}\mu\text{m}$  peak in CU Cep and the  $9.4\text{-}\mu\text{m}$  bands in HL Tau and Elias 7 could be partially crystalline hydrous silicates with spectral signatures similar to the CIT mixture. The spectrum of Elias 16 is too noisy to diagnose the

presence of a CIT band in quiescent TMC dust, but it does contain the  $10.4\text{-}\mu\text{m}$  band indicative of serpentine (Paper I). In contrast the CIT band is absent from the dry diffuse medium towards Cyg OB2 no. 12 and the dominant fine structure there is the ubiquitous  $8.9\text{--}9.2 \mu\text{m}$  band identified with crystalline pyroxenes, serpentines (and possibly silicas which have weaker  $9.2\text{-}\mu\text{m}$  bands than those of Ferraro's specimens). Serpentines may contribute to the Cyg OB2 no. 12 profile since the match between 10 and  $10.4 \mu\text{m}$  is marginally better for mixture V (mixture II excluding CIT minerals) than for mixture III (Tables 2 and 3). The absence of a narrow  $11.2\text{-}\mu\text{m}$  band in any of the astronomical residuals indicates that crystalline olivine *does not* contribute significantly to these spectra. Unshaded boxes highlight bands that are most similar to those of mixed crystalline pyroxenes.

We infer (i) that hydrous silicates may exist in environments with high abundances of  $\text{H}_2\text{O}$  in the form of vapour or ice, but that hydrous silicates are absent from the dry diffuse medium towards Cyg OB2 no. 12, and (ii) that the abundance of crystalline olivine in these environments is insufficient to produce an  $11.2\text{-}\mu\text{m}$  feature in either emission or absorption.

## 6 DISCUSSION

### 6.1 Silicon abundance and silicate stoichiometry

In all cases modelling the spectra with mixtures including crystalline silicates substantially decreases the number of silicon atoms required. In the circumstellar environments of CU Cep and U Aur the reduction is 52 and 29 per cent respectively, in the diffuse medium the reduction is 37 per cent, and in the TMC and YSOs it is 46 per cent. For the diffuse medium towards  $\zeta$  Ophiuchi the gas-phase depletion of silicon is 17 Si per  $10^6$  hydrogen atoms (Snow & Witt 1996). The canonical value for the hydrogen atom is  $5.8 \times 10^{21}$  H atoms/unit of  $E(B - V)$ , and the standard ratio of total to selective extinction is 3.1, which provides  $1.9 \times 10^{22}$  hydrogen atoms. Therefore mixture III requires 39 Si per  $10^6$  hydrogen atoms, i.e. 2.3 times the ideal number.

The stoichiometry of the preferred matches, mixtures I, III and IV listed in Table 4, indicates that, for each Si atom, 1.0–1.3 metal atoms are required, with the amount of metal decreasing with the age of the silicate. If in astronomical silicates  $\text{Mg}/\text{Fe} > 0.90$ , as it is in GEMS and interplanetary dust particles (IDPs) (Bradley et al.

<sup>4</sup>The near-infrared data for hydrous silicates were obtained from KBr spectra published by Fiveash Data Management, Inc.

<sup>5</sup>Filio et al. (1994) conducted X-ray diffraction (XRD) and radial distribution function (RDF) studies of talc ground in tumbling and planetary ball mills. After  $\geq 2$  h of dry grinding, XRD analysis indicated a glass-like disordered structure. RDF indicated an increase in Si–Si, Si–Mg and Mg–Mg pairs, i.e. a breakdown of the silicate sheets and disordering in the metal ion and hydroxyl layers.

1999a,b) and is indicated by the *ISO* spectra of astronomical silicate dust (e.g. Malfait et al. 1998; Bowey et al. 2002), then the Mg:Si ratio of 1.1:1.3 indicates that nearly all the cosmically depleted Mg is taken up in silicates. The total oxygen content included in silicates decreases from 3.5 to 3.1 atoms per Si between mixtures I and IV. However, most of the loss is because 0.54 of the oxygen atoms are locked up in the hydroxyl ions. The oxygen content associated with the silicate anions increases with the larger pyroxene content in agreement with the amorphous hypothesis that the oxygen content of the silicates increases with the degree of processing.

### 6.1.1 Ratio of H<sub>2</sub>O ice to silicate column density

The H<sub>2</sub>O ice abundances based on the optical depth of the 3.05- $\mu$ m

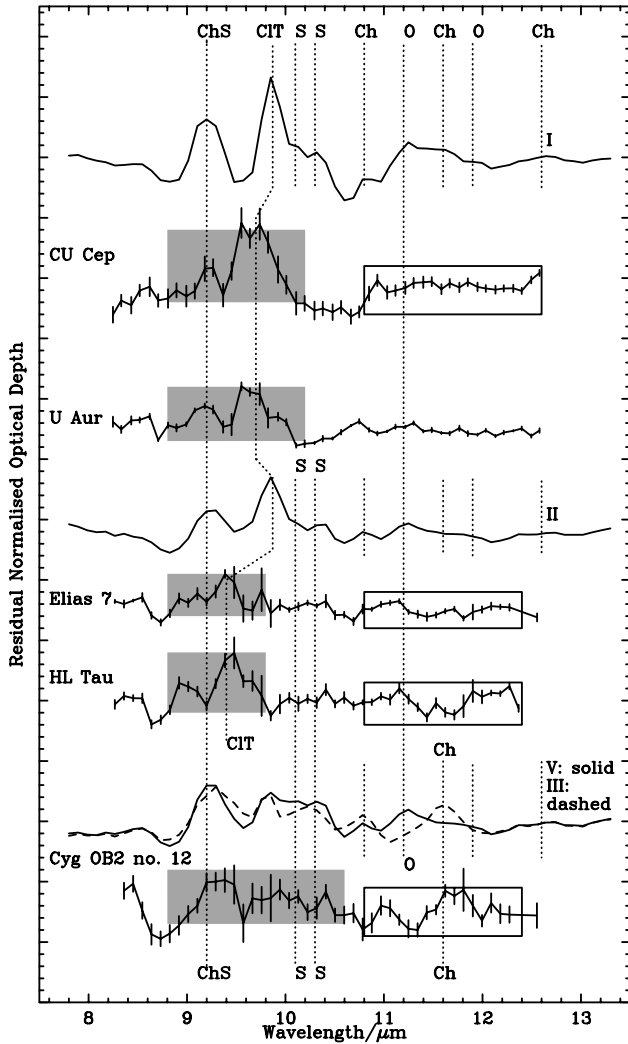


**Figure 7.** Fine structure in the observations and laboratory averages. Residuals were obtained by subtracting a smoothed spectrum (shown in Fig. 2) from each of the normalized 10- $\mu$ m emissivities. The y-axis has been arbitrarily offset; major intervals = 0.1. Fine structures in the laboratory residuals of mixtures I, II, III and V are due to: olivines (O), pyroxenes (Ch), clays and talc (CIT), serpentines (S). Shaded boxes: 9.4–9.8  $\mu$ m peak, hydrous talc/clay-like silicates; 9.0–9.2  $\mu$ m bump, pyroxenes, serpentines or silicas (silicas are not included in the laboratory mixtures). Open boxes: structure tentatively identified with pyroxenes; in the case of CU Cep, pyroxenes are required to fit the wing longwards of 10.8  $\mu$ m (see Section 5).

ice band in the lines of sight to the TMC sources and towards Cyg OB2 no. 12 were given in Table 1. The ratio,  $N_{\text{H}_2\text{O}}/N_{\text{Si-O}}$  for the preferred silicate mixtures for the silicate absorption profiles is < 2 per cent for Cyg OB2 no. 12, and 63, 24 and 9 per cent for Elias 16, HL Tau and Elias 7, respectively; in the amorphous silicate interpretation these ratios are halved. In the TMC the change in the ratio of the water ice to silicate column densities correlates with the amount of silicate emission in each environment, since Elias 16 is a field star with only cold foreground dust, HL Tau has optically thin silicate emission local to the source and Elias 7 silicate emission is optically thick.

## 6.2 Mass fractions

The mass fractions of crystalline silicate in the mixtures which best match the overall profiles are startlingly large; a substantial fraction of crystalline pyroxene is required in all sampled lines of sight (see Tables 4 and 5).

The fraction of crystalline pyroxene increases with the FWHM of the profile and the degree of processing from  $\sim$ 40 per cent in CU Cep to  $\sim$ 80 per cent in the Taurus molecular-cloud and YSO environments. In the circumstellar environment of CU Cep the silicates may be entirely crystalline (mixture I). By mass, the respective fractions of crystalline olivine, pyroxene, serpentine and CIT minerals are 25, 39, 25 and 11 per cent. In this hydrous environment,  $\sim$ 36 per cent of the silicate mass could be due to phyllosilicates, and even though there is no apparent 11.2- $\mu$ m olivine band in the spectrum a quarter of the mass is in olivines. Fits to the circumstellar profile of U Aur require 60 per cent crystalline pyroxene and 40 per cent amorphous silicate. Comparison of the fine structures with the differences between the spectra of mixtures I and II (which contains 16 per cent by mass of amorphous silicate, the remainder being due to mixture I) suggests that  $\sim$ 5 per cent of this circumstellar dust could be due to a CIT mineral.

However, there is no evidence for this type of phyllosilicate in the low-density interstellar environment towards Cyg OB2 no. 12, which is well matched by mixture III. Mixture V, which includes 20 per cent serpentine, is a good match to the fine structure near 10.4  $\mu$ m but a poor match to the overall profile (compare Figs 5 and 6), and therefore we expect the contribution of serpentine to the spectrum to be a few per cent at most. Fits to the profiles of TMC and YSO dust consist of 17 per cent amorphous and 83 per cent crystalline pyroxene. However, the fine structures in the profiles may indicate that  $\sim$ 5 per cent of the dust is similar to a CIT mineral. One might also expect olivines to be present, but the 11.2- $\mu$ m band is hidden in these 10- $\mu$ m spectra. If crystalline olivine exists in the diffuse ISM and the quiescent TMC, olivine bands should be present in far-infrared spectra. The feature is also absent from the YSO spectra even though far-infrared forsterite bands have been observed in the high-mass YSOs HD 100546 and MWC 922 (e.g. Malfait et al. 1998; Bowey et al. 2002). Future spectropolarimetric observations may reveal the 11.2- $\mu$ m feature of aligned olivine grains in other YSO and some interstellar environments.

## 7 CONCLUSIONS

We interpret the 10- $\mu$ m profiles of silicates in a wide variety of galactic environments (newly formed O-rich circumstellar dust, dust in the diffuse medium, and silicates in quiescent and YSO regions of the Taurus molecular cloud) in terms of a mixed

crystalline and amorphous mineralogy. Since the sensitivity of ISO's SWS and LWS spectrometers was insufficient to obtain good spectra of cold molecular-cloud and diffuse-medium silicates, we await new observations with the IRS on *SIRTf* before extending this analysis into the far-infrared.

A mixed mineralogy is simulated by averaging laboratory spectra of crystalline and amorphous silicates; since the Si–O stretch is common to all silicates, the narrow bands of crystalline grains could blend to form the observed astronomical 10- $\mu\text{m}$  profiles. For *all* the environments studied here, including the diffuse ISM,  $\chi^2/n$  of spectral matches are significantly improved (by factors of 1.3–4.0) if crystalline silicates are included in the mixture. In addition the number of silicon atoms required to model the spectra decreases by 30–50 per cent if crystalline silicates are included in the mixture.

Changes in the wavelength of the 10- $\mu\text{m}$  peak (Pégourié & Papoular 1985) and increases in bandwidth indicate that Taurus molecular-cloud (TMC) dust is richer in amorphous and crystalline pyroxene than are circumstellar and diffuse-medium dust, which contains more olivine. Upper limits to the mass fraction of crystalline pyroxene increase with the FWHM of the profile, from  $\sim 50$  per cent in the sampled circumstellar environments to  $\sim 80$  per cent in the Taurus molecular cloud and its embedded YSOs.

Fine structures common to both the averaged spectra of laboratory silicates and astronomical profiles suggest that  $\leq 10$  per cent by mass of the silicates in circumstellar and star-forming environments rich in H<sub>2</sub>O vapour or ice could be partially crystalline hydrous (i.e. OH<sup>−</sup> containing) silicates similar to clays like talc and montmorillonite, but that these grains are absent from the dry UV-rich diffuse medium towards Cyg OB2 no. 12. In contrast, the relative abundance of submicrometre-sized crystalline olivine is insufficient ( $\leq 25$  per cent) in these circumstellar, diffuse-medium, molecular-cloud and YSO spectra to produce an 11.2- $\mu\text{m}$  emission or absorption feature. Using this method of spectral analysis, the mass fraction of amorphous silicate in these spectra could be as low as 17 per cent in the TMC and 0 per cent in some circumstellar environments.

More observations and laboratory experiments are required to verify the uniqueness of the fits and these hypotheses. It may be possible to distinguish mineral components in 10- $\mu\text{m}$  data by obtaining long-slit spectra across circumstellar envelopes with 8-m telescopes. Another method that shows promise for separating mineral components is 10- $\mu\text{m}$  spectropolarimetry. The lack of observations is particularly severe for lines of sight through the diffuse-medium and quiescent molecular-cloud environments, for which the included 'high signal-to-noise ratio' 10- $\mu\text{m}$  spectra of dust towards Cyg OB2 no. 12 and Taurus-Elias 16, respectively, are the only good data. No good spectra of these environments exist longwards of 13  $\mu\text{m}$ .

## ACKNOWLEDGMENTS

The work reported herein is based on observations with CGS3 at the UK Infrared Telescope (UKIRT). The authors would like to thank the anonymous referee for his/her constructive and knowledgeable reports, which have improved this paper. The hypotheses of a mixed crystalline/amorphous silicate mineralogy and the possibility of a hydrous silicate component were presented in JEB's PhD thesis (dated 1998 October). JEB was funded by a University of Central Lancashire studentship, A. L. Woodcraft and PPARC post-doctoral positions at Queen Mary and Westfield College London and University College London. AJA was funded

by the UK Starlink project, the University of Central Lancashire and PPARC.

## REFERENCES

- Aitken D. K., Roche P. F., Smith C. H., Hough J. H., 1988, MNRAS, 230, 629
- Anders E., Grevesse N., 1989, Geochim. Cosmochim. Acta, 53, 197
- Bernstein M. P., Sandford S. A., Allamandola L. J., Chang S., Scharberg M. A., 1995, ApJ, 454, 327
- Blanco A., Fonti S., Martino M., Bussoletti E., Mennella V., Colangeli L., Stephens J. R., 1993, in Kwok S., ed., ASP Conf. Ser. Vol. 41, Astronomical Infrared Spectroscopy: Future Observational Directions. Astron. Soc. Pac., San Francisco, p. 267
- Bowey J. E., Adamson A. J., 2001, MNRAS, 320, 131 (Paper II)
- Bowey J. E., Adamson A. J., Whittet D. C. B., 1998, MNRAS, 298, 131 (Paper I)
- Bowey J. E., Adamson A. J., Speck A. K., 2000, in Sitko M. L., Sprague A. L., Lynch D. K., eds, ASP Conf. Ser. Vol. 196, Thermal Emission Spectroscopy and Analysis of Dust, Disks, and Regoliths. Astron. Soc. Pac., San Francisco, p. 31
- Bowey J. E., Lee C., Tucker C., Hofmeister A. M., Ade P. A. R., Barlow M. J., 2001, MNRAS, 325, 886
- Bowey J. E. et al., 2002, MNRAS, 331, L1
- Bradley J. P. et al., 1999a, Sci, 285, 1716
- Bradley J. P., Snow T. P., Brownlee D. E., Hanner M. S., 1999b, in d'Hendecourt L., Joblin C., Jones A., eds, Les Houches No. 11, Solid Interstellar Matter: The ISO Revolution. EDP Sciences, Les Ulis, p. 297
- Cesarsky D., Jones A. P., Lequeux J., Verstraete L., 2000, A&A, 358, 708
- Chiar J.-E., Adamson A.-J., Kerr T.-H., Whittet D. C. B., 1995, ApJ, 455, 234
- Draine B. T., Lee H. M., 1984, ApJ, 285, 89
- Fabian D., Henning T., Jäger C., Mutschke H., Dorschner J., Wehrhan O., 2001, A&A, 378, 228
- Farmer V. C., 1958, Mineral. Mag., 31, 829
- Ferraro J. R., 1982, The Sadtler Infrared Spectra Handbook of Minerals and Clays. Sadtler Research Laboratories
- Filio J. M., Kazumasa S., Saito F., Waseda Y., 1994, Powder Technology, 78, 121
- Forrest W. J., Gillett F. C., Stein W. A., 1975, ApJ, 195, 423
- Gail H.-P., Sedlmayr E., 1986, A&A, 166, 225
- Hanner M. S., Brooke T. Y., Tokunaga A. T., 1995, ApJ, 438, 250
- Hanner M. S., Brooke T. Y., Tokunaga A. T., 1998, ApJ, 502, 871
- Hofmeister A. M., Keppel E., Bowey J. E., Speck A. K., 2000, ESA, SP-456, 343
- Hudgins D. M., Sandford S. A., Allamandola L. J., Tielens A. G. G. M., 1993, ApJS, 86, 713
- Jäger C., Mutschke H., Begemann B., Dorschner J., Henning Th., 1994, A&A, 292, 641
- Koike C., Shibai H., 1994, MNRAS, 269, 1011
- Koike C., Tsuchiyama A., 1992, MNRAS, 255, 248
- Koike C., Hasegawa H., Hattori T., 1982, Ap&SS, 88, 89
- Koike C., Shibai H., Tsuchiyama A., 1993, MNRAS, 264, 654
- Koike C. et al., 2000, A&A, 363, 1115
- Lacy J. H., Faraji H., Sandford S. A., Allamandola L. J., 1998, ApJ, 501, L105
- Malfait K., Waelkens C., Waters L. B. F. M., Vandenbussche B., Huygen E., de Graauw M. S., 1998, A&A, 332, L25
- Monnier J. D., Geballe T. R., Danchi W. C., 1998, ApJ, 502, 833
- Nuth J. A., Donn B., Nelson R., 1986, ApJ, 310, L83
- Ossenkopf V., Henning T., Mathis J. S., 1992, A&A, 261, 567
- Pégourié B., Papoular R., 1985, A&A, 142, 451
- Russell R. W., Soifer B. T., Forrest W. J., 1975, ApJ, 198, L41
- Skinner C. J., Tielens A. G. G. M., Barlow M. J., Justanont K., 1992, ApJ, 399, L79
- Smith C. H., Wright C. M., Aitken D. K., Roche P. F., Hough J. H., 2000, MNRAS, 312, 327
- Snow T. P., Witt A. N., 1996, ApJ, 468, L65
- Speck A. K., Hofmeister A. M., Barlow M. J., 1999, ApJ, 513, L87

- Speck A. K., Barlow M. J., Sylvester R. J., Hofmeister A. M., 2000, *A&AS*, 146, 437
- Stephens J. R., Blanco A., Bussoletti E., Colangeli L., Fonti S., Mennella V., Orofino V., 1995, *Planetary Space Sci.*, 43, 1241
- Waters L. B. F. M. et al., 1996, *A&A*, 315, L361
- Whittet D. C. B., 1992, *Dust in the Galactic Environment*. IOP Publishing, Bristol
- Whittet D. C. B. et al., 1988, *MNRAS*, 233, 321
- Whittet D. C. B. et al., 1997, *ApJ*, 490, 729
- Wooden D. H., Harker D. E., Woodward C. E., Butner H. M., Koike C., Witteborn F. C., McMurtry C. W., 1999, *ApJ*, 517, 1034

## APPENDIX A: CALCULATION OF MASS ABSORPTION COEFFICIENT, INTEGRATED CROSS-SECTION AND MASS FRACTION FOR CRYSTALLINE MIXTURES

### A1 Estimate of mass absorption coefficient, $\kappa(\lambda)$

For each mineral class we adopt a measurement of the mass absorption coefficient of a single mineral at the wavelength of the Si–O peak for the class (see Table 3). The contrast in the 10- $\mu\text{m}$  optical depth spectra of individual minerals in the Ferraro (1982) and Koike catalogues (Koike et al. 1982; Koike & Tsuchiyama 1992; Koike et al. 1993; Koike & Shibai 1994; Koike et al. 2000) is the same to  $\leq 5$  per cent. Differences between members within a group are accounted for in equation (2).

Each mixture of  $n$  minerals is composed of  $n_j$  minerals from spectral class  $j$  for which  $\kappa_j$  is the mass absorption coefficient of the class at wavelength  $\lambda$ . Hence,  $\bar{\kappa}$ , the mass absorption coefficient of the mixture listed in Table 3, is given by

$$\bar{\kappa}(\lambda) \approx \frac{1}{n} \sum_j n_j \kappa_j(\lambda_{\text{pk } j}) \times \frac{\tau_j(\lambda)}{\tau_j(\lambda_{\text{pk } j})}. \quad (\text{A1})$$

### A2 Estimates of integrated cross-section, $\sigma_{\text{int}}$ , and mass fraction, $m_{r j}$

For each spectral class, the integrated cross-section of the band per

Si–O bond,  $\sigma_{\text{int}}$  (Table 3), was obtained by multiplying the area of the optical depth spectrum,  $A_{\text{sil}}$  by the ratio of the mean relative molecular mass,  $\bar{m}_r$ , to the number of Si–O bonds,  $Z \times r_{\text{O:Si}}$ , for a mole of silicon atoms, where  $Z$  is Avogadro’s number and  $r_{\text{O:Si}}$  is the ratio of oxygen to silicon in the silicate anion, i.e.

$$\sigma_{\text{int } j} = A_{\text{sil } j} \frac{\bar{m}_r j}{Z r_{\text{O:Si } j}}, \quad (\text{A2})$$

where  $A_{\text{sil } j}$  is the area of the unnormalized peak. Since the profiles are not Gaussian, it is inappropriate to use the FWHM and optical depth of the feature to obtain an integrated band strength. Therefore,

$$A_{\text{sil } j} = \bar{\kappa}_j(\lambda_{\text{pk } j}) \int_{7.8}^{13.3} \bar{\tau}_j(\lambda) d\lambda. \quad (\text{A3})$$

For a crystalline mixture including several classes the mean integrated cross-section is

$$\bar{\sigma}_{\text{int}} = \frac{1}{n} \sum_j \sigma_{\text{int } j}, \quad (\text{A4})$$

and the mass fraction,  $m_{r j}$ , of each mineral component is given by

$$m_{r j} = f_j m_{r j} / m_{r \text{ mix}}, \quad (\text{A5})$$

where  $f_j$  is the integrated cross-section due to each component:

$$f_j = \frac{n_j \sigma_{\text{int } j}}{n \bar{\tau}_{\text{pk}} \hat{\sigma}_{\text{int}}}, \quad (\text{A6})$$

and  $\hat{\sigma}_{\text{int}}$  is the integrated cross-section of the normalized average spectrum of the mixture. The mass fractions and stoichiometries of the mineral components and mixtures are given in Table 4.

This paper has been typeset from a  $\text{\TeX}/\text{\LaTeX}$  file prepared by the author.